Water Science and Engineering, 2009, 2(3): 37-47
doi:10.3882/j.issn.1674-2370.2009.03.004

http://kkb.hhu.edu.cn
e-mail: wse@hhu.edu.cn

Application of 2-D sediment model to fluctuating backwater area of Yangtze River

Yong FAN*

College of Water Conservancy and Hydropower Engineering, Hohai University, Nanjing 210098, P. R. China

Abstract: Based on the characteristics of backflow, a two-dimensional mathematical model of sediment movement was established. The complexity of the watercourse boundary at the confluence of the main stream and the tributary was dealt with using a boundary-fitting orthogonal coordinate system. The basic equation of the two-dimensional total sediment load model, the numerical calculation format, and key problems associated with using the orthogonal curvilinear coordinate system were discussed. Water and sediment flow in the Chongqing reach of the Yangtze River were simulated. The calculated water level, flow velocity distribution, amount of silting and scouring, and alluvial distribution are found to be in agreement with the measured data, which indicates that the numerical model and calculation method are reasonable. The model can be used for calculation of flow in a relatively complicated river network.

Key words: *fluctuating backwater area; 2-D numerical simulation; sediment carrying capacity; Yangtze River; suspended load; bed load*

1 Introduction

The development of sediment transport models has always lagged behind that of the numerical hydrodynamic models on which they are based. The modern sediment transport model was developed at the end of the 1970s. Demuren and Rodi (1986) used the κ-ε turbulence model to simulate the movement of a tracer in a curved conduit. Later, Demuren (1989) expanded this model and applied it to the simulation of suspended load transport. Demuren (1991) created another bed load transport model and calculated the flow and sediment movement in a curved water tank to verify the experimental results of Odgaard and Bergs (1988). Shimizu and Yamaguchi (1990) calculated the flow and riverbed deformation of tortuous channels based on a simplified three-dimensional sediment model. Lin and Falconer (1996) created a model to simulate the floating debris movement in an estuary region. Based on the FAST3D flow pattern, Wu et al. (2000) developed a three-dimensional total load transport formula. Olsen and Kjellesvig (1998) developed a three-dimensional numerical model for a sedimentation basin. In addition, Fang and Wang (2000) developed a three-dimensional numerical model based on non-orthogonal curvilinear grids to simulate

This work was supported by the National Natural Science Foundation of China (Grant No. 50879006).
*Corresponding author (e-mail: *fyhhu@126.com*)
Received Jun. 13, 2009; accepted Aug. 17, 2009

turbulent secondary flow and movement of floating debris. Yang and Lim (2003) derived a total load transport formula suitable for alluvial channels based on experimental data. Yang (2005) also analyzed the correlation between the sediment transport rate and the flow factor, and derived a formula suitable for calculating the sediment transport rate in channels, estuaries and coastal areas. Sarmiento and Falcon (2006) arrived at the features and concrete expression of dimensionless shear stress for uniform sediment based on theoretical research and experimental analysis.

The inflow of tributaries, especially those tributaries with a large area and abundant water and sediment, significantly affects the flow and sediment movement in main streams that have many tributaries. The flood periods of the main stream are different from those of the tributaries, and there is an interaction between their water levels. The decreases of the flow velocity cause decreases in the sediment carrying capacity of the current, leading to a great amount of sediment deposition and the formation of shoals in the tributary estuary, and further affecting shipping on the main stream and tributaries. The serious sediment deposition in the fluctuating backwater area also leads to the formation of alluvial regions along the banks. Ports have to be abandoned and navigation channels in the upper region of the fluctuating backwater area deteriorate. If the amount of incoming sediment of the upper reach changes, corresponding changes will occur in the sediment deposition in the fluctuating backwater area. Suitable measures should be taken to deal with different sediment conditions. Therefore, it is necessary to study the influence of sediment deposition on the port and navigation channels as well as corresponding treatment measures in fluctuating backwater areas. Such research would have significant economical and social benefits.

2 Numerical models

2.1 Governing equations

The governing equations of the two-dimensional mathematical model of sediment movement in the body-fitted orthogonal curvilinear coordinate system are as follows:

(1) The continuity equation of the current is

$$\frac{\partial H}{\partial t}+\frac{1}{C_\xi C_\eta}\frac{\partial}{\partial \xi}\left(huC_\eta\right)+\frac{1}{C_\xi C_\eta}\frac{\partial}{\partial \eta}\left(hvC_\xi\right)=0 \tag{1}$$

where ξ and η are the two orthogonal curvilinear coordinates in the orthogonal curvilinear coordinate system; u and v are the flow velocities in the ξ and η directions, respectively; h is the water depth; H is the water level; and C_ξ and C_η are the viscous Lame coefficients in the orthogonal curvilinear coordinate system.

The momentum equation in the ξ direction is

$$\frac{\partial u}{\partial t}+\frac{1}{C_\xi C_\eta}\left[\frac{\partial}{\partial \xi}\left(C_\eta u^2\right)+\frac{\partial}{\partial \eta}\left(C_\xi vu\right)+vu\frac{\partial C_\eta}{\partial \eta}-v^2\frac{\partial C_\eta}{\partial \xi}\right]=-g\frac{1}{C_\xi}\frac{\partial H}{\partial \xi}-$$
$$\frac{u\sqrt{u^2+v^2}n^2g}{h^{4/3}}+\frac{1}{C_\xi C_\eta}\left[\frac{\partial}{\partial \xi}\left(C_\eta \sigma_{\xi\xi}\right)+\frac{\partial}{\partial \eta}\left(C_\xi \sigma_{\eta\xi}\right)+\sigma_{\xi\eta}\frac{\partial C_\xi}{\partial \eta}-\sigma_{\eta\eta}\frac{\partial C_\eta}{\partial \xi}\right] \tag{2}$$

The momentum equation in the η direction is

$$\frac{\partial v}{\partial t}+\frac{1}{C_\xi C_\eta}\left[\frac{\partial}{\partial \xi}\left(C_\eta vu\right)+\frac{\partial}{\partial \eta}\left(C_\xi v^2\right)+uv\frac{\partial C_\eta}{\partial \xi}-u^2\frac{\partial C_\xi}{\partial \eta}\right]=-g\frac{1}{C_\eta}\frac{\partial H}{\partial \eta}-$$
$$\frac{v\sqrt{u^2+v^2}n^2g}{h^{4/3}}+\frac{1}{C_\xi C_\eta}\left[\frac{\partial}{\partial \xi}\left(C_\eta \sigma_{\xi\eta}\right)+\frac{\partial}{\partial \eta}\left(C_\xi \sigma_{\eta\eta}\right)+\sigma_{\eta\xi}\frac{\partial C_\eta}{\partial \xi}-\sigma_{\xi\xi}\frac{\partial C_\xi}{\partial \eta}\right] \tag{3}$$

where n is the roughness coefficient, g is the acceleration of gravity; and $\sigma_{\xi\xi}$, $\sigma_{\xi\eta}$, $\sigma_{\eta\xi}$, and $\sigma_{\eta\eta}$ are the turbulent stresses:

$$\sigma_{\xi\xi}=2\nu_t\left(\frac{1}{C_\xi}\frac{\partial u}{\partial \xi}+\frac{v}{C_\xi C_\eta}\frac{\partial C_\xi}{\partial \eta}\right),\quad \sigma_{\eta\eta}=2\nu_t\left(\frac{1}{C_\eta}\frac{\partial v}{\partial \eta}+\frac{u}{C_\xi C_\eta}\frac{\partial C_\eta}{\partial \xi}\right),\text{ and}$$

$$\sigma_{\xi\eta}=\sigma_{\eta\xi}=\nu_t\left[\frac{C_\eta}{C_\xi}\frac{\partial}{\partial \xi}\left(\frac{v}{C_\eta}\right)+\frac{C_\xi}{C_\eta}\frac{\partial}{\partial \eta}\left(\frac{u}{C_\xi}\right)\right].$$

The turbulent viscous coefficient ν_t in above equations is generally defined as $\nu_t=\alpha u_* h$, where u_* is the shear velocity, which is defined by the von Karman-Prandt logarithmic velocity profile, $u_*=\kappa u'/\ln(z/z_0)$; κ is the von Karman constant (≈ 0.40); u' is the near-bed velocity; z is the depth at the center of the bottommost layer; and the parameter z_0 is the local roughness height at the bottom.

(2) The non-equilibrium sediment transport equation for suspended loads is derived as follows: According to granular sizes, a non-uniform suspended load can be divided into n_0 groups. Dou Guoren's two-dimensional non-equilibrium sediment transport equation for the sediment content of group L in a non-uniform suspended load is

$$\frac{\partial hS_L}{\partial t}+\frac{1}{C_\xi C_\eta}\left[\frac{\partial}{\partial \xi}\left(C_\eta huS_L\right)+\frac{\partial}{\partial \eta}\left(C_\xi hvS_L\right)\right]=$$
$$\frac{1}{C_\xi C_\eta}\left[\frac{\partial}{\partial \xi}\left(\frac{\varepsilon_\xi}{\sigma_s}\frac{C_\eta}{C_\xi}\frac{\partial hS_L}{\partial \xi}\right)+\frac{\partial}{\partial \eta}\left(\frac{\varepsilon_\eta}{\sigma_s}\frac{C_\xi}{C_\eta}\frac{\partial hS_L}{\partial \eta}\right)\right]+\alpha_L\omega_L\left(S_L^*-S_L\right) \tag{4}$$

where S_L is the sediment content of group L in the suspended load, defined as $S_L=P_{SL}S$; P_{SL} is the ratio of the sediment content of corresponding granular size in the suspended load; S is the total sediment content of the suspended load; S_L^* is the sediment carrying capacity of group L, defined as $S_L^*=P_{SL}^*S^*$; P_{SL}^* is the gradation of the sediment carrying capacity of group L; the sediment carrying capacity of the current, $S^*=\left[\sum_{L=1}^{n_0}\frac{P_{SL}}{S_L^*}\right]^{-1}=K_0\left[\frac{\left(u^2+v^2\right)^{3/2}}{h}\right]^m\sum_{L=1}^{n_0}\frac{P_{SL}}{\omega_L^m}$; ω_L is the settling velocity of the sediment of group L; α_L is the recovery saturation coefficient of

sediment content of group L, which is 0.5 during silting, and ranges from 0.5 to 1.0 during scouring; K_0 is the coefficient of sediment carrying capacity; m is the power exponent, set as 1/6; ε_ξ and ε_η are the sediment diffusion coefficients in the ξ and η directions; and σ_s is the model calibration parameter, defined as $\sigma_s = 1$.

(3) The non-equilibrium sediment transport equation for bed loads is as follows: According to granular sizes, a non-uniform bed load can be divided into n_0 groups. Dou Guoren's two-dimensional non-equilibrium sediment transport equation for bed loads is

$$\begin{aligned}&\frac{\partial hS_{bL}}{\partial t}+\frac{1}{C_\xi C_\eta}\left[\frac{\partial}{\partial \xi}\left(C_\eta huS_{bL}\right)+\frac{\partial}{\partial \eta}\left(C_\xi hvS_{bL}\right)\right]=\\&\frac{1}{C_\xi C_\eta}\left[\frac{\partial}{\partial \xi}\left(\frac{\varepsilon_\xi}{\sigma_b}\frac{C_\eta}{C_\xi}\frac{\partial hS_{bL}}{\partial \xi}\right)+\frac{\partial}{\partial \eta}\left(\frac{\varepsilon_\eta}{\sigma_b}\frac{C_\xi}{C_\eta}\frac{\partial hS_{bL}}{\partial \eta}\right)\right]+\alpha_{bL}\omega_{bL}\left(S_{bL}^*-S_{bL}\right)\end{aligned} \tag{5}$$

where S_{bL}^* is the sediment carrying capacity of group L in the bed load; S_{bL} is the sediment content of the bed load layer; α_{bL} is the recovery saturation coefficient of group L in the bed load; ω_{bL} is the settling velocity of group L in the bed load; and σ_b =1.

(4) The equation of bed load gradation, which expands the one-dimensional model of the CARICHAR mixing layer into a two-dimensional model, is

$$\gamma_s\ \frac{\partial E_m P_{mL}}{\partial t}+\alpha_L\omega_L\left(S_L-S_L^*\right)+\alpha_{bL}\omega_{bL}\left(S_{bL}-S_{bL}^*\right)+\left[\varepsilon_1 P_{mL}+\left(1-\varepsilon_1\right)P'_{mL}\right]\gamma_s\ \left(\frac{\partial Z}{\partial t}-\frac{\partial E_m}{\partial t}\right)=0 \tag{6}$$

where P_{mL} and P'_{mL} are the initial bed load gradation in and under the mixing layer of the riverbed, respectively; E_m is the thickness of the mixing layer; Z is the riverbed elevation; and γ_s is the bed material dry density. The physical meaning of the fourth item at the left-hand side of Eq. (6) is the replenishment to the mixing layer by the riverbed, which results from the continuous cutting of the riverbed during the scouring of the lower interface of the mixing layer. In this way, there still remains sufficient sediment although a large amount of sediment has been scoured in the mixing layer. ε_1 is 0 when the original riverbed is affected by the scouring in the mixing layer; otherwise, it is 1.

(5) The riverbed deformation equation (Dou 1983) is

$$\gamma_s\ \frac{\partial Z}{\partial t}=\alpha_L\omega_L\left(S_L-S_L^*\right)+\alpha_{bL}\omega_{bL}\left(S_{bL}-S_{bL}^*\right) \tag{7}$$

2.2 Numerical computation model and numerical solution

Comparing Eqs. (1) through (5), we find that they have a similar form, so a universal format for Eqs. (1) through (5) is provided:

$$C_\xi C_\eta\frac{\partial \psi}{\partial t}+\frac{\partial\left(C_\eta u\psi\right)}{\partial \xi}+\frac{\partial\left(C_\xi v\psi\right)}{\partial \eta}=\frac{\partial}{\partial \xi}\left(\Gamma\frac{C_\eta}{C_\xi}\frac{\partial \psi}{\partial \xi}\right)+\frac{\partial}{\partial \eta}\left(\Gamma\frac{C_\xi}{C_\eta}\frac{\partial \psi}{\partial \eta}\right)+C \tag{8}$$

where ψ is the flux, which represents h, u, v, hS_L, and hS_{bL} in Eqs.(1) through (5), respectively; Γ is the diffusion coefficient; and C is the source item. In this way, Eqs. (1)

through (5) can be standardized according to Eq. (8). During numerical calculation, the compilation of only one universal program for Eq. (8) can solve Eqs. (1) through (5). The control volume method is used for discretizing Eq. (8). In order to overcome the difficulty of discretizing the pressure gradient and continuity equation, the staggered grid method is adopted, and the power function is used for discretizing the convection-diffusion item. In addition, from Eq. (8) and all governing equations, we can see that the main difference in all the equations is in the source items. The source items are the functions of dependent variables. To accelerate the convergence in computation, the source items of all equations are linearized with a negative gradient coefficient. The tridiagonal matrix algorithm is used to solve the differential equation row by row. The SIMPLEC program proposed by Partaker and Spalding is used for the entire numerical computation. To avoid divergence caused by truncation error of the computer, the under-relaxation method is used in the numerical computation. The convergence standard is that the ratio of the residual mass source to the inlet mass flow in the continuity equation should be less than 0.5%.

2.3 Boundary conditions and movable boundary technique

Flux, sediment content and sediment gradation at the inlet are given, and water level processes are given as the exit boundary. Non-slip conditions are adopted for the bank boundary; that is to say, the inshore velocity is zero.

The movable boundary technique is adopted if the boundaries of a point bar and channel bar vary with the fluctuation of water levels. The dry-wet condition of a grid cell is determined based on the comparison between the calculated water level and the riverbed elevation at the water level node. If the grid cell is below the water surface, the roughness coefficient n will be assigned a normal value; otherwise, a very large positive value, such as 10^{30}, will be assigned to it. When using the momentum equation to compute the flow velocity at four sides of the exposed cell, the average roughness coefficient of adjacent nodes can be used as its roughness coefficient. Whether the adjacent cells are exposed or not, the average resistance will always be a maximum value. Therefore, as compared with the item of resistance, other items in the momentum equation are infinitesimal. The calculation results of the flow velocity at the four sides of the exposed cell must be infinitesimal. To continue the computation, the water depth of the exposed cell is set as 0.005 m (Da Silva 1995).

3 Application of 2-D sediment mathematical model

The simulation of current and sediment deposition was validated for the Chongqing reach of the upper Yangtze River from Qiezixi (687.6 km from Yichang) to Tongluoxia (644 km from Yichang) and for a reach of 25 km from Shimen to the Jialingjiang Estuary (Fig. 1).

3.1 Hydrology and sediment data

The Changjiang Waterway Bureau surveyed the landforms of the entire river reach in

January and November of 1986. Flood deposition landforms in the Shimen wide and shallow section of Jialingjiang River, near Jinshaozi in the Jialingjiang Estuary, and in the Jiulongtan wide and shallow sections of the Yangtze River were surveyed in September. At the same time, the instantaneous flow profile, flow velocity, sediment content, sediment gradation, and distribution of the bed load transport rate along the river width were measured. The observed fluxes at Cuntan Station on the Yangtze River were, respectively, 3 170 m^3/s, 6 400 m^3/s, and 22 600 m^3/s on March 8, November 22, and September 22 of 1986, and, simultaneously, the fluxes at Beibei Station on the Jialingjiang River were 447 m^3/s, 716 m^3/s, and 1 710 m^3/s. Sampling analysis of the bed load was conducted during the dry season.

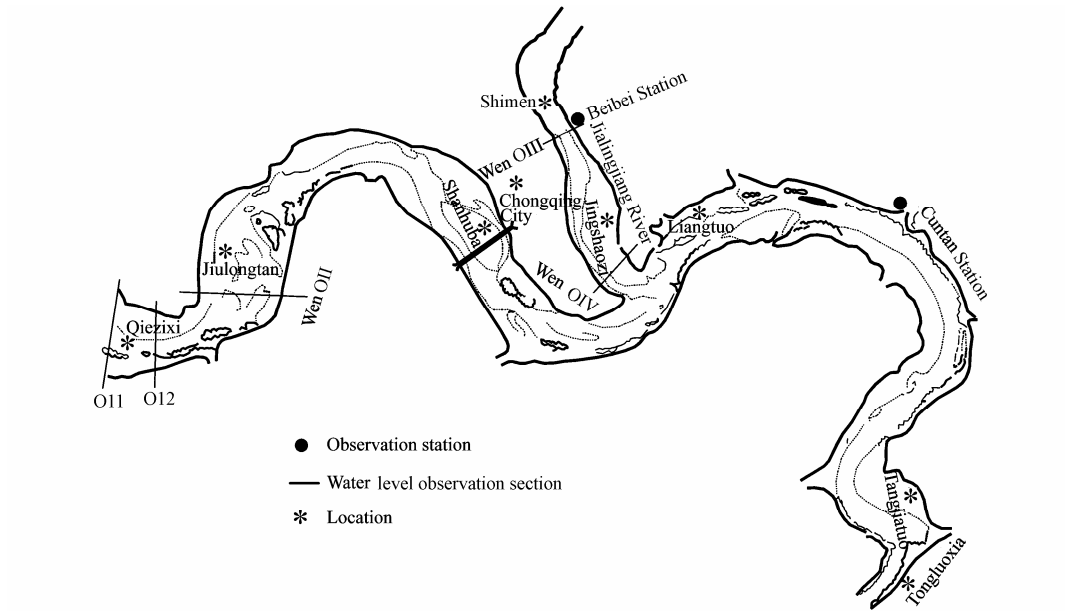

Fig. 1 River regime of Chongqing reach

3.2 Calculation regions and generation of orthogonal curvilinear grids

There were 407 × 63 grid points in the two calculation regions mentioned above. There were 248 × 31 grid points from Qiezixi on the Yangtze River to the confluence of the Jialingjiang River and Yangtze River, 248 × 31 grid points for the Jialingjiang River, and 159 × 63 grid points from the confluence to Tongluoxia. Orthogonal curvilinear grids were obtained after orthogonal calculation. Except for some individual points on the bank, the intersection angles of the grid nodes all ranged from 88° to 92°, and orthogonality was basically maintained. The spaces between orthogonal curve grids were 80 m to 120 m along the longitudinal direction of the river and 10 m to 40 m along the transverse direction of the river.

3.3 Water level validation

On November 22, 1986, the flux was 6 400 m^3/s at Cuntan Station and 716 m^3/s at Beibei Station. Except at some individual water gauges, the differences between calculated instantaneous

water levels along the watercourse and the measured data were less than 0.1 m. The roughness coefficients of various river reaches, at corresponding fluxes, are given in Table 1.

Table 1 Comparison of calculated and measured water levels on November 22, 1986

River reach	Serial number of observation section	Mileage (km)	Water level (m)			Roughness coefficient
			Calculated	Measured	Error	
Qiezixi to Tongluoxia	O11	686.6(1)	169.821	169.800	0.021	0.028
	O12	679.4(1)	167.869	167.800	0.069	0.034
	Wen OII	673.9(1)	166.024	165.950	0.074	0.026
Shimen to Jialingjiang Estuary	Wen OIII	7.5(2)	162.175	162.110	0.065	0.022
	Wen OIV	30.0(2)	158.975	159.032	−0.057	0.022

Note: (1) means that the mileage is the distance from Tongluoxia; (2) means that the mileage is the distance from Shimen.

3.4 Validation of flow velocity distribution

Comparisons between the calculated results and measured data of flow velocity (V) and sediment content (c) at Cuntan Station with the fluxes of 6 400 m^3/s and 22 600 m^3/s are given in Fig. 2. The measured riverbed elevation of the Cuntan section in January of 1986 is given in Fig. 3. The calculated results are in good agreement with the measured data. The average flow velocity in the Cuntan section was 1.4 m/s when the flux at Cuntan Station was 6 400 m^3/s, and it was unevenly distributed along the section (Fig. 2(a)). At this time, the flux at the Jialingjiang Estuary was 716 m^3/s, and the confluence ratio R was 0.11. When the flux at Cuntan Station was 22 600 m^3/s, the flow velocity in the deep trough was 2.85 m/s, and the average flow velocity in the section was 2.2 m/s (Fig. 2(b)). At this time, the flux at the Jialingjiang Estuary was 1 710 m^3/s, the confluence ratio R was 0.076, and the flow velocity was unevenly distributed along the section. The flow velocity distribution along the Cuntan section, with a high velocity in large, deep troughs and low velocity at point bars, fully reflects the effects of river topography. What needs to be pointed out is that, being affected by the current of the Yangtze River, the flow velocity at the Wen OIII section was only 0.5 m/s.

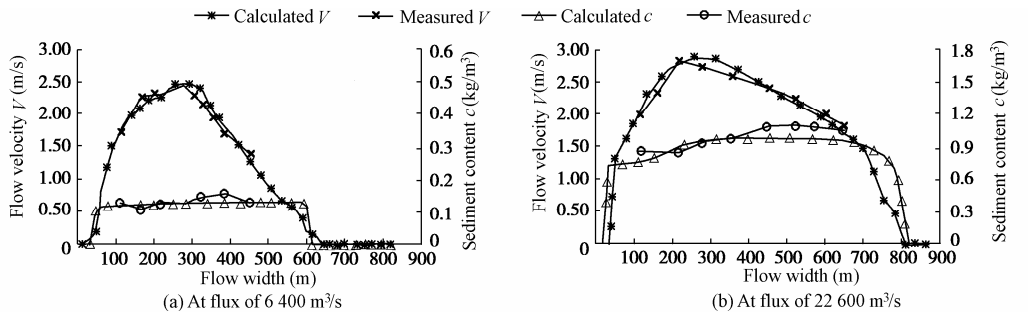

Fig. 2 Comparison of calculated and measured results of flow velocity and sediment content in Cuntan section

3.5 Validation of riverbed deposition

The riverbed alluvium validation period was from the middle of January to the middle of November, 1986. In total, 88 time intervals were divided: five to six days were set as the time

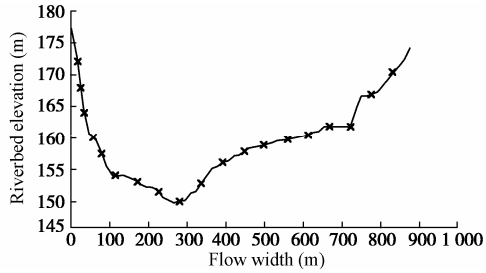

Fig. 3 Measured riverbed elevation of Cuntan section in January of 1986

interval in the non-flood season, and one to two days were set as the time interval in the flood season. The suspended sediment concentration of six particle size groups was calculated. The annual average value of the proportion of different particle sizes was used in the calculation. The percentage and settling velocity of suspended sediment of different particle sizes at the inlet of the Yangtze River and the Jianglingjiang River are listed in Table 2. The sediment transport rates of seven particle size groups in the bed load were calculated, and the distribution of particle sizes of sediment in the bed load ranged from 1 mm to 200 mm. The percentages of different particle size groups at Cuntan Station were 0.83%, 9.47%, 38.00%, 24.40%, 13.30%, 10.90%, and 2.80%, respectively, for the particle sizes 1-10 mm, 10-20 mm, 20-50 mm, 50-75mm, 75-100 mm, 100-150 mm, and 150-200 mm. The transport rate of the pebble bed load with particle sizes ranging from 10 mm to 200 mm was calculated with the empirical formula obtained from measured data by the Nanjing Hydraulic Research Institute, which is

$$g_b = 8.0 \times 10^{-12} \beta Q^{2.60} \tag{9}$$

where g_b is the bed load transport rate; β is the efficiency coefficient, defined as $\beta = 11.6$; and Q is the flux. Due to the lack of measured pebble bed load data from the Jialingjiang River, the pebble bed load sediment transport rate of the Jialingjiang River was estimated through comparison of its flux with the main stream flux in the calculation. The gravel bed load with particles ranging in size from 1 mm to 10 mm was considered 3% of the pebble bed load, while the bed load with particle sizes less than 1 mm was considered the suspended load in the calculation. The thickness of the mixing layer E_m is related to the bed sand characteristics. E_m was estimated as being from 1.0 m to 2.0 m for a gravel riverbed, and from 2.0 to 3.0 m for a sandy riverbed. The latter was roughly equivalent to the height of a sand wave.

Table 2 Gradation and settling velocity of suspended sediment of different particle sizes at inlet

Particle size (mm)	Proportion of different size groups (%)		Settling velocity (mm/s)
	Yangtze River	Jialingjiang River	
0.005 0	23.6	17.7	0.016
0.016 9	20.9	19.9	0.018
0.036 8	25.9	28.9	0.855
0.073 6	17.6	24.1	3.390
0.169 0	8.0	7.0	16.400
0.368 0	4.0	2.4	51.100

The amounts of silting and scouring of two reaches were simulated:

(1) The Shimen reach: Located 20-22 km upstream of the Jialingjiang Estuary, the width of the widest and shallowest part of the Shimen reach is twice that of the deep channel section in the upper reach. The flow velocity and sediment carrying capacity of the current in the wide section are far less than those in the deep channel section of the upper reach. This leads to a large amount of silting during the water-rising period in the wide section. During the water-falling period, water flows into the deep channel, the flow velocity increases, the sediment that accumulated during the flood season is scoured, and the topography of the riverbed basically returns to what it was during the low water period. The calculated and measured silting and scouring areas from March to September of 1986 are provided in Fig. 4.

(2) Jiulongtan reach of the Yangtze River: The Jiulongtan reach is 669-674 km upstream of Yichang City. The sudden widening of the river reach, the reduction of the flow velocity, and the weakening of the sediment carrying capacity cause silting during the flood season. The calculated and measured alluvial distributions from March to September of 1986 are shown in Fig. 5. The turbulence of the current is largely due to a bend of the watercourse and the strong diffusion and convection in the Jiulongtan reach, so the distribution of silting areas is decentralized.

The calculated and measured amounts of souring and silting for the Shimen reach and Jiulongtan reach are compared in Table 3. From Fig. 4, Fig. 5 and Table 3, we can see that the calculated alluvial distribution and sediment amount are relatively close to the measured data, and the silting mainly occurred at the bends, rough parts of the bank, backflow areas, and wide and shallow reaches of the watercourse. After the silting process, the shoreline of the riverbed became smoother.

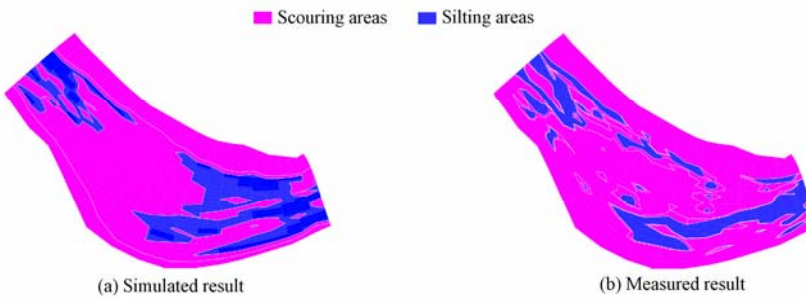

Fig. 4 Alluvial distribution of Shimen reach from March to September of 1986

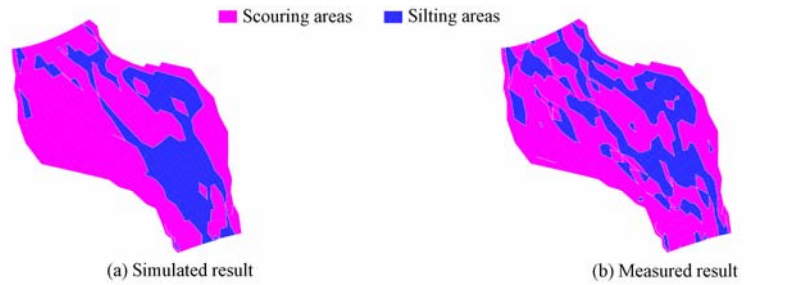

Fig. 5 Alluvial distribution of Jiulongtan reach from March to September of 1986

Table 3 Comparison of calculated and measured silting and scouring amounts in river reaches

River reach	Amount of silting (10^4 m^3) (Mar.-Sep., 1986)		Amount of scouring (10^4 m^3) (Sep.-Nov., 1986)	
	Calculated	Measured	Calculated	Measured
Jiulongtan	187.4	181.7	−97.0	−115.2
Shimen	20.0	23.1	−11.5	−11.6

4 Conclusions

A two-dimensional mathematical model was established to simulate the water and sediment movement in a fluctuating backwater area of the Chongqing reach of the upper Yangtze River. The complexity of the watercourse boundary at the confluence of the main stream and tributaries was dealt with using a boundary-fitting orthogonal coordinate system. The basic equation of the two-dimensional total sediment load model, the numerical calculation format, and key problems associated with the use of the orthogonal curvilinear coordinate system were discussed. Water and sediment simulation, including the water level, flow velocity distribution, silting and scouring amount, and alluvial distribution, was performed for the Chongqing reach of the Yangtze River. Simulated results show that the characteristics of currents in backwater areas are complicated. A large flow velocity gradient exists around the confluence of the main stream with the tributary due to their interaction. The flow velocity distribution, with high velocities in large, deep troughs and low velocities at point bars, reflects the effects of river topography. In backflow areas, the silting mainly occurred at bends, rough parts of the bank, and wide and shallow reaches of the watercourse. The shoreline of the riverbed became smoother after the silting process.

The agreement between the simulated results and measured data indicates that the numerical model and its calculation method are reasonable. The model can be used for the calculation of relatively complicated river networks. The simulation and analysis of the water flow characteristics in the backflow area have theoretical significance for backwater flow research and practical significance for engineering application.

References

Da Silva, A. 1995. *Turbulent Flow in Sine-Generated Meandering Channel*. Ph. D. Dissertation. Kingston: Queen's University.

Demuren, A. O., and Rodi, W. 1986. Calculation of flow and pollutant dispersion in meandering channels. *Journal of Fluid Mechanics*, 172, 63-92. [doi:10.1017/S0022112086001659]

Demuren, A. O. 1989. Calculation of sediment transport in meandering channels. *Proceedings of 23rd IAHR Congress: Tech Session A*. Delft: International Association for Hydraulic Research.

Demuren, A. O. 1991. *Development of a Mathematical Model for Sediment Transport in Meandering Rivers, Report 693*. Karlsruhe: Institute for Hydromechanics, University of Karlsruhe.

Dou, G. R. 1983. *Similarity Theory of Total Sediment Transport Modeling for Estuarine and Coastal Regions*. Nanjing: River and Harbor Engineering Department, Nanjing Hydraulic Research Institute. (in Chinese)

Fang, H. W., and Wang, G. Q. 2000. Three-dimensional mathematical model of suspended-sediment transport. *Journal of Hydraulic Engineering*, 126(8), 578-592. [doi:10.1061/(ASCE)0733-9429(2000)126:8(578)]

Lin, B. L., and Falconer, R. A. 1996. Numerical modeling of three-dimensional suspended sediment for

estuarine and coastal waters. *Journal of Hydraulic Research*, 34(4), 435-456.

Odgaard, A. J, and Bergs, M. A. 1988. Flow processes in a curved alluvial channel. *Water Resources Research*, 24(1), 45-56.

Olsen, N. R. B., and Kjellesvig, H. M. 1998. Three-dimensional numerical flow modeling for simulation of maximum local scour depth. *Journal of Hydraulic Research*, 36(4), 579-597.

Sarmiento, O. A., and Falcon, M. A. 2006. Critical bed shear stress for unisize sediment. *Journal of Hydraulic Engineering*, 132(2), 172-179. [doi:10.1061/(ASCE)0733-9429(2006)132:2(172)]

Shimizu, Y., and Yamaguchi, H. 1990. Three-dimensional computation of flow and bed deformation. *Journal of Hydraulic Engineering*, 116(9), 1090-1108. [doi:10.1061/(ASCE)0733-9429(1990)116:9(1090)]

Wu, W. M., Rodi, W., and Wenka, T. 2000. 3D numerical modeing of flow and sediment transport in open channels. *Journal of Hydraulic Engineering*, 26(1), 4-15. [doi:10.1061/(ASCE)0733-9429(2000) 126:1(4)]

Yang, S. Q., and Lim, S. Y. 2003. Total load transport formula for flow in alluvial channels. *Journal of Hydraulic Engineering*, 129(1), 68-72. [doi:10.1061/(ASCE)0733-9429(2003)129:1(68)]

Yang, S. Q., 2005. Formula for sediment transport in rivers, estuaries, and coastal waters. *Journal of Hydraulic Engineering*, 131(11), 968-979. [doi:10.1061/(ASCE)0733-9429(2005)131:11(968)]